Scripta Materialia 134 (2017) 61–65

Contents lists available at ScienceDirect

Scripta Materialia

journal homepage: www.elsevier.com/locate/scriptamat

Regular Article

A pathway to microstructural refinement through double pulsed gas metal arc welding

L.L. Wang [a], H.L. Wei [b], J.X. Xue [a], T. DebRoy [b,*]

[a] School of Mechanical and Automotive Engineering, South China University of Technology, Guangzhou 510641, China
[b] Department of Materials Science and Engineering, The Pennsylvania State University, University Park, PA 16802, USA

ARTICLE INFO

Article history:
Received 15 January 2017
Received in revised form 18 February 2017
Accepted 20 February 2017
Available online xxxx

Keywords:
Double pulsed welding
Modeling
Microstructure
Grain refining

ABSTRACT

In fusion welding, variations of cooling rate and microstructure are commonly achieved by changing heat input. Here we show that the cooling rates can be adjusted and microstructural features could be refined at constant heat input while changing the pulsing parameters. The temporal variations of cooling rates, solidification growth rate and weld geometry during both single and double pulsed welding of an aluminum alloy are examined. Furthermore, microstructures of both single and double pulsed gas metal arc welding are presented to demonstrate significant microstructural refinement of double pulsed gas metal arc welds for the same heat input.

Aluminum alloys are joined by friction stir welding or fusion welding depending on applications [1–4]. For the welding of many intricate parts, gas metal arc welding still remains a widely used process of choice [5]. Defect free, structurally sound and reliable welds can be achieved economically by pulsed gas metal arc welding. Single pulsed gas metal arc welding (SP-GMAW) and double pulsed gas metal arc welding (DP-GMAW) are two important fusion welding methods for the joining of aluminum alloys. Achieving a desired microstructure remains an important goal in fusion welding of aluminum alloys.

Here we show that the adjustment of pulsing parameters through the use of DP-GMAW provides a means to control the heating and cooling processes and achieves a refined microstructure. The benefits of using DP-GMAW over SP-GMAW include reduced incidence of porosity in the weld metal [6,7], better ability to bridge the gaps in the butting surfaces particularly in large components [8] and better ability to control the mode of droplet transfer [9], all of which affect the structure and properties of welds.

DP-GMAW is characterized by its special current waveform which provides significant process flexibility and control over that can be attained by the conventional SP-GMAW. Fig. 1 schematically illustrates the current waveform and the temporal variations of the transverse and the longitudinal sections of the welds produced by DP-GMAW. The welding current used during DP-GMAW is characterized by its pulsed waveform in two sets of pulsing frequencies. Typically, the high pulsing frequency is on the order of 100 Hz and the low pulsing frequency is about 1–5 Hz. The high pulsing frequency is designed to achieve controllable droplet transfer to the liquid metal pool. The low pulsing frequency allows control of the heating and cooling processes during DP-GMAW [10].

Periodic variations of fusion zone geometry, peak temperature, cooling rate and solidification parameters occur during DP-GMAW due to time dependent heat input and these variations significantly affect the microstructure of the weld metal. What is necessary and not available in the literature is a rigorous understanding of how and why the bead geometry and microstructure attained by DP-GMAW evolve with time and differ from those produced by SP-GMAW. In this work, the temporal variations of cooling rate, solidification growth rate and weld geometry were calculated using a three-dimensional heat transfer and fluid flow model to correlate these parameters with the scale of microstructures in aluminum alloy 6061 for DP-GMAW and SP-GMAW.

Bead-on-plate welding experiments were carried out on aluminum alloy AA6061 base metal ($200 \times 80 \times 4$ mm^3) using ER4043 filler wire. Chemical compositions of alloys AA6061 and ER4043 are presented in Table 1 [11]. Process parameters of SP-GMAW and DP-GMAW are presented in Table 2. Pure argon was coaxially supplied as shielding gas at a flow rate of 18 L/min. After welding, specimens were cut along transverse and longitudinal cross sections of welds. The samples were ground and polished to 0.06 um using colloidal silica, which were subsequently etched using the standard Keller agent with 10 s for metallographic analysis. The secondary dendrite arm spacing was measured in three locations of both SP-GMA and DP-GMA welds. Each location contained more than six secondary dendrites.

* Corresponding author.
E-mail address: rtd1@psu.edu (T. DebRoy).

http://dx.doi.org/10.1016/j.scriptamat.2017.02.034
1359-6462/

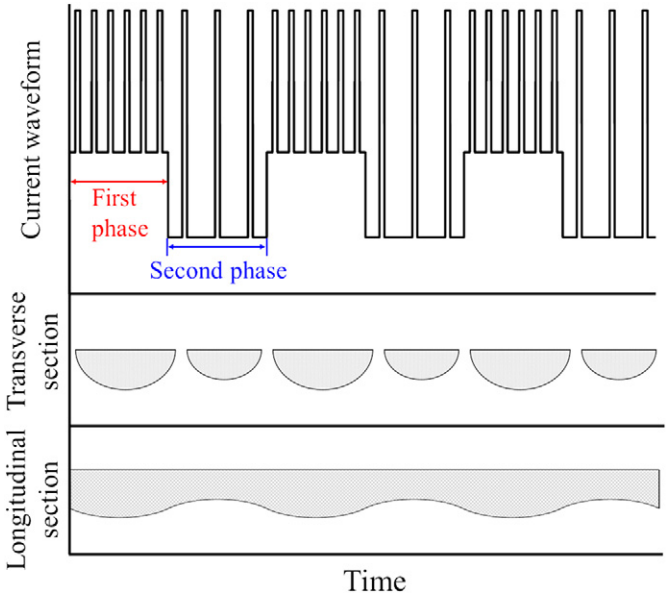

Fig. 1. Schematic diagram of current waveform and transverse and longitudinal sections of the DP-GMAW weld pool.

The temperature and velocity fields were calculated using a well-tested, transient, three-dimensional heat transfer and fluid flow model that solves the equations of conservation of mass, momentum and energy. The metal transfer mode during SP-GMAW and DP-GMAW is droplet transfer with one droplet per high frequency pulse. A volumetric heat source is incorporated in the model to account for the energy transferred by the overheated droplets into the weld pool [12,13]. Details of the governing equations and boundary conditions can be found in our previous papers and are not repeated here [14–18]. The thermophysical properties used in the heat transfer and fluid flow model are presented in Table 3 [19,20].

The pulsing current of SP-GMAW in the model is implemented as constant mean current of 100 A. Such a simplification offers enhanced computational efficiency without affecting the accuracy of the calculations. The current pulsing frequency of SP-GMAW was 100 Hz and under such high frequency the weld pool behaves similar to the case of constant current welding [21]. The experimentally observed results show that the weld pool geometry is constant during SP-GMAW [22]. The currents during the first and the second pulse phases of DP-GMAW, 140 A and 60 A, respectively, are implemented in a similar way to that for SP-GMAW.

The temperature gradient (G), growth rate (R) and their combined form GR which represents cooling rate are important solidification parameters. The parameters G and R are temporally and spatially variable and they can be calculated from the heat transfer and fluid flow calculations. The value R was calculated at the trailing edge of the melt pool on the top surface using the following relation:

$$R = \frac{\Delta d_s}{\Delta t} \tag{1}$$

where Δd_s is the displacement of the trailing edge during a short time interval of Δt. The cooling rate was calculated near the bottom of the weld pool to match the location for microstructure evaluation.

Table 1
Chemical compositions of AA6061 and ER4043 (wt%) [11].

Material	Mg	Si	Fe	Cu	Mn	Cr	Al
AA6061	1.02	0.75	0.45	0.25	0.06	0.05	Bal.
ER4043	0.05	5.60	0.80	0.30	0.05	–	Bal.

Table 2
Welding process parameters for SP-GMAW and DP-GMAW.

Process parameters	SP-GMAW	DP-GMAW
Mean voltage (V)	22.3	22.3
Mean current (A)	100	100
Welding speed (mm/s)	8	8
Wire feeding rate (mm/s)	62	62
Wire diameter (mm)	1.2	1.2
Density of wire (kg/m^3)	2685	2685
Frequency (Hz)	100	2.5
First phase current (A)	–	140
Second phase current (A)	–	60
First phase time (s)	–	0.2
Second phase time (s)	–	0.2

Fig. 2 (a), (b) and (c) shows the calculated temperature and velocity fields in the transverse sections of SP-GMAW and DP-GMAW, respectively. In all cases, the liquid metal flows from the center to the periphery of the melt pool near the top surface driven by Marangoni stress due to the spatial gradient of surface tension. In the molten weld pool, the liquid metal circulates with velocities of about 300 mm/s. At these high velocities, heat is transported mainly by convection within the melt pool. In addition, the size of the SP-GMAW weld pool lies between the largest and the smallest sizes of the weld pools formed by DP-GMAW for the same heat input. The finger penetration characteristic of GMA welding is observed in Fig. 2 (a), (b) and (c). Although the mean current is low for both SP-GMAW and DP-GMAW, the peak current reaches 300 A. The filler wire is rapidly melted and a droplet is generated for each pulse when the peak current is applied. The overheated droplets are accelerated by the electromagnetic force and impinge into the weld pool at a high speed. The resulting transport of heat to the interior of the weld pool causes finger penetration. It can be observed from Fig. 2 (a), (b) and (c) that the calculated results match well with the experimental data.

The depths of penetration of DP-GMAW welds vary with time in a periodic manner as shown in Fig. 2 (e), which is consistent with the temporal variation of heat input. This pattern differs significantly from the constant penetration depth of SP-GMAW shown in Fig. 2 (d). The maximum and minimum penetration depths are attained after 1.4 s at the end of first pulsing phase and 1.6 s at the end of the second pulsing phase, respectively. An important feature of DP-GMAW is that the peak temperature in the melt pool changes periodically whereas it is constant during SP-GMAW as shown in Fig. 3 (a). Another important outcome of the time dependent heat input during DP-GMAW is the periodic shrinkage and expansion of the melt pool. This variation leads to unusual remelting and resolidification of the weld metal. It will be shown subsequently that the unusual temporal variations of the melt pool geometry and cooling rate during DP-GMAW result in a unique solidification

Table 3
Data used for the calculations [19,20].

Variables and unit	Value
Density of liquid metal (kg m^{-3})	2400
Viscosity of liquid (kg m^{-1} s^{-1})	0.001
Solidus temperature (K)	855
Liquidus temperature (K)	925
Enthalpy of solid at melting point (J kg^{-1})	0.596
Enthalpy of liquid at melting point (J kg^{-1})	0.981
Specific heat of solid (J kg^{-1} K^{-1})	980
Specific heat of liquid (J kg^{-1} K^{-1})	1160
Thermal conductivity of solid (W m^{-1} K^{-1})	168
Thermal conductivity of liquid (W m^{-1} K^{-1})	108
Coefficient of thermal expansion (K^{-1})	2.375×10^{-5}
Temperature coefficient of surface tension (N m^{-1} K^{-1})	-3.5×10^{-4}

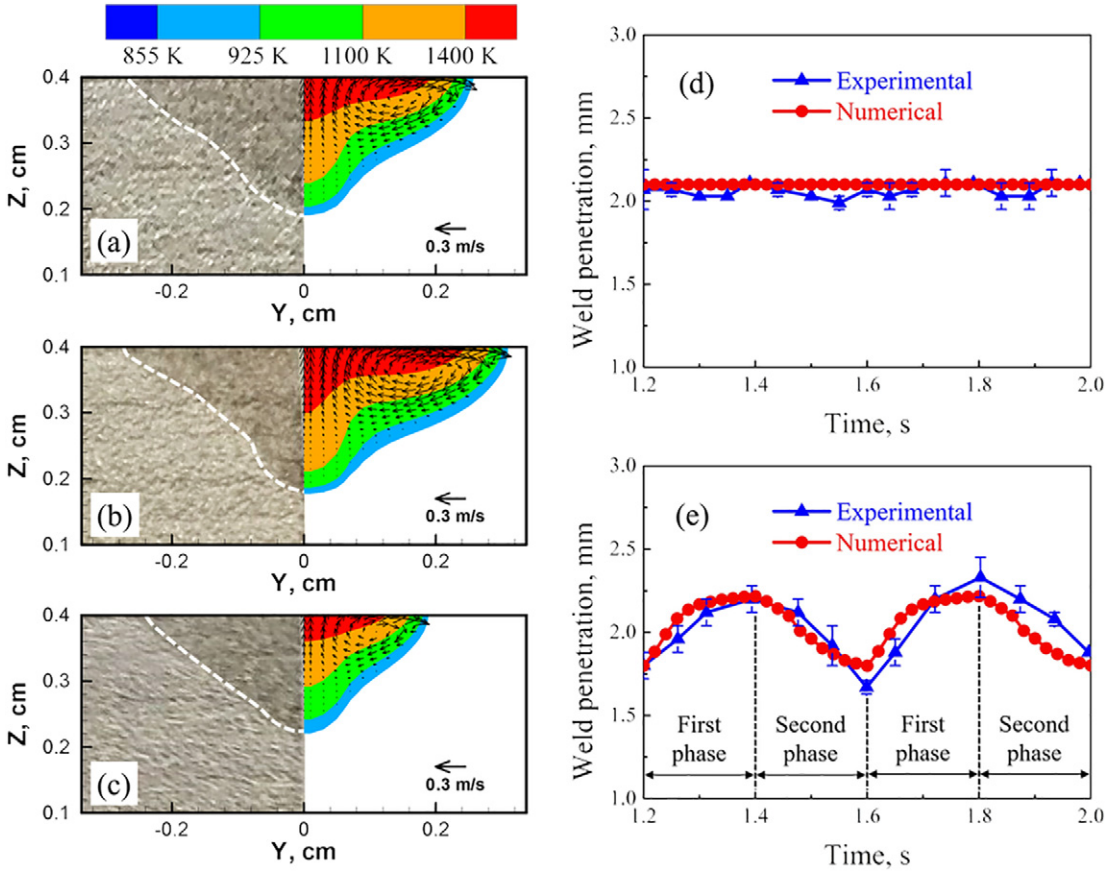

Fig. 2. (a) Transverse section of the SP-GMAW weld. (b) Largest transverse section of the DP-GMAW weld. (c) Smallest transverse section of the DP-GMAW weld. (d) Weld penetration depth versus time of the SP-GMAW weld. (e) Weld penetration depth versus time of the DP-GMAW.

condition and microstructure that are significantly different from those attained by SP-GMAW.

The calculated temporal variation of solidification growth rate, R, at the trailing edge of the weld pool is shown in Fig. 3 (b). Unlike SP-GMAW, R is time dependent for DP-GMAW. It can be observed from Fig. 3 (b) that during the first phase of pulsing that lasts from 1.2 to 1.4 s, the solidification growth rate R decreases with time from 1.2 to 1.3 s. This is because the melt pool expands from 1.2 to 1.3 s, with its trailing edge moving in a direction opposite to the welding direction. Despite the constant welding speed, the trailing edge comes to a standstill with R decreasing to 0 mm/s at 1.24 s, which means that the expansion speed of the melt pool at its trailing edge is equal to the welding speed. The growth rate is negative between 1.24 and 1.3 s because the expansion speed of the melt pool is higher than the welding speed. A remelting of the previously solidified weld metal occurs during this time, which is a strikingly different behavior from that in SP-GMAW. On the other hand, R increases from 1.3 to 1.4 s due to the lower expansion speed of the melt pool compared with the welding speed.

Solidification growth rate at the trailing edge of the weld pool, R, increases rapidly from 1.4 to 1.5 s within the second pulsing phase which spans from 1.4 to 1.6 s. The higher growth rate originates from the significant shrinkage of the melt pool during this period. The overall growth rate is the sum of the shrinkage and welding speeds since both displacements are in the same direction. After the maximum shrinkage velocity is reached at 1.5 s, the growth rate decreases from 1.5 to 1.6 s. The mean value of the solidification growth rate, R, is 10.8 mm/s for the DP-GMAW welds. This value is greater than the constant R of SP-GMAW which is 8.0 mm/s.

Fig. 3 (c) shows the variation of cooling rate with time near the bottom of the weld pool. The mean value of cooling rate for DP-GMAW, 1735 K/s, is significantly higher than the 1330 K/s rate for SP-GMAW. The mean value of the cooling rate of DP-GMAW was calculated from the variable data in Fig. 3 (c). The difference in the cooling rates of the two processes affects the scale of microstructures of the welds.

Note that the scale of the solidification structure is significantly affected by the cooling rate. The relation between the secondary dendrite arm spacing (λ_2) and cooling rate (GR) is given as [23,24]:

$$\lambda_2 = a(GR)^{-n} \tag{2}$$

Where the exponent n lies between 1/3 and 1/2, and a is a constant whose value depends on the alloy system. Eq. (2) indicates that the secondary dendrite arm spacing decreases with increase in cooling rate. The refined solidification structure of welds fabricated by DP-GMAW originates from the higher cooling rate.

Fig. 4 shows the microstructures from the transverse sections of the welds by SP-GMAW and DP-GMAW. They were taken from the same position within the welds for a meaningful comparison as indicated by the insert. Additionally, the microstructures and cooling rates are evaluated at the same location which is at the bottom of the weld pool. As expected, the microstructures featured an Al-Si eutectic phase distributed within the α-Al matrix [25]. Cellular structures were observed near the fusion line, which developed into columnar dendrites further away from the fusion line. The cell spacings produced by DP-GMAW were significantly smaller than that within the microstructure produced by SP-GMAW. The measured secondary dendrite arm spacings were 13.4 ± 2.3 μm and 10.2 ± 0.8 μm for SP-GMAW and DP-GMAW, respectively, consistent with finer solidification structure in DP-GMAW for identical mean heat input for the two processes.

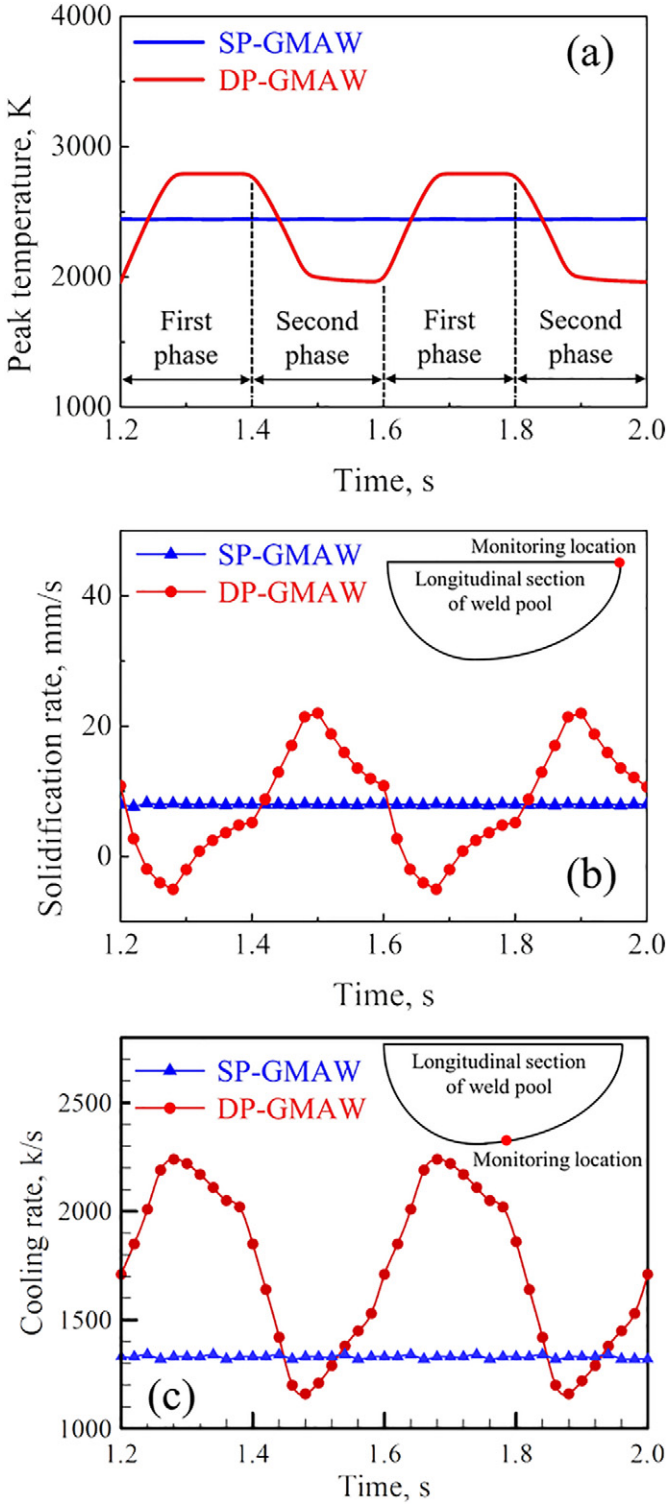

Fig. 3. Calculated temporal variations of (a) peak temperature, (b) solidification rate and (c) cooling rate.

In summary, double and single pulsed gas metal arc welding of aluminum alloy 6061 were studied both experimentally and theoretically. The periodic shrinkage and expansion of the melt pool during double pulsed welding led to an unusual remelting and resolidification behavior of the weld metal. Solidification rates and cooling rates were significantly higher for the double pulsed gas metal arc welding than those for the single pulsed welding and these differences were responsible for the significant refinement of microstructure during double pulsed welding.

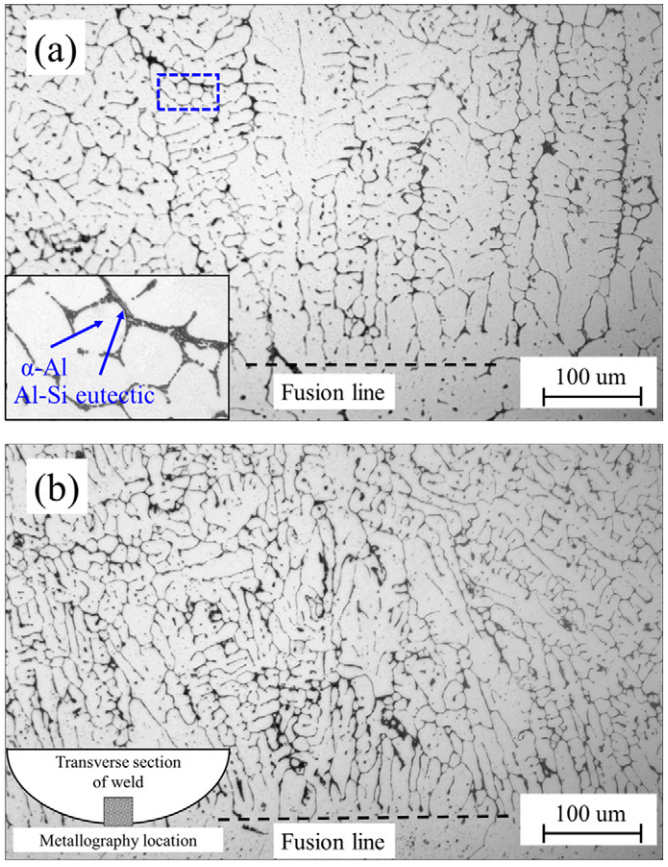

Fig. 4. Microstructures of 6061 aluminum alloy welds showing a darker Al-Si eutectic phase distributed within the lighter α-Al matrix. (a) SP-GMAW and (b) DP-GMAW.

We thank James S. Zuback for his help in preparing the metallographic specimens. One of the authors acknowledges financial support for this research from the High-level Leading Talent Introduction Program of GDAS (2016GDASRC-0106); Industry-university-research Program of Guangdong Province and the Ministry of Education (2013B090600098, 2013B090600030); and the SCUT Doctoral Student Short-Term Overseas Visiting Study Funding Project.

Appendix A. Supplementary data

Supplementary data to this article can be found online at http://dx.doi.org/10.1016/j.scriptamat.2017.02.034.

References

[1] U. Donatus, G.E. Thompson, X. Zhou, Scr. Mater. 123 (2016) 126–129.
[2] T. DebRoy, H.K.D.H. Bhadeshia, Sci. Technol. Weld. Join. 15 (2010) 266–270.
[3] R. Nandan, T. DebRoy, H.K.D.H. Bhadeshia, Prog. Mater. Sci. 53 (2008) 980–1023.
[4] A. Elrefaey, Sci. Technol. Weld. Join. 20 (2015) 280–285.
[5] P.L. Threadgill, A.J. Leonard, H.R. Shercliff, P.J. Withers, Int. Mater. Rev. 54 (2009) 49–93.
[6] C.L.M. da Silva, A. Scotti, J. Mater. Process. Technol. 171 (2006) 366–372.
[7] L.L. Wang, G.C. Heng, H. Chen, J.X. Xue, F.L. Lin, W.J. Huang, Int. J. Adv. Manuf. Technol. 86 (2016) 1841–1851.
[8] H. Yamamoto, S. Harada, T. Ueyama, S. Ogawa, Weld. Int. 6 (1992) 580–583.
[9] A. Liu, X. Tang, F. Lu, Mater. Des. 50 (2013) 149–155.
[10] L.L. Wang, L. Jin, W.J. Huang, M. Xu, J.X. Xue, Mater. Manuf. Process. 31 (2016) 2152–2157.
[11] D. Bardel, M. Fontaine, T. Chaise, M. Perez, D. Nelias, F. Bourlier, J. Garnier, Acta Mater. 117 (2016) 81–90.
[12] C.H. Kim, W. Zhang, T. DebRoy, J. Appl. Phys. 94 (2003) 2667–2679.
[13] D.V. Kiran, J. Cheon, N. Arif, H. Chung, S.-J. Na, Int. J. Adv. Manuf. Technol. 86 (2016) 1453–1474.
[14] H.L. Wei, J.W. Elmer, T. DebRoy, Acta Mater. 115 (2016) 123–131.
[15] H.L. Wei, J.J. Blecher, T.A. Palmer, T. Debroy, Weld. J. 94 (2015) 135S–144S.
[16] A. De, T. DebRoy, Weld. J. 84 (2005) 101S–112S.

[17] S. Mishra, T. DebRoy, J. Appl. Phys. 98 (2005), 044902. .
[18] S. Mishra, T.J. Lienert, M.Q. Johnson, T. DebRoy, Acta Mater. 56 (2008) 2133–2146.
[19] H. Zhao, T. Debroy, Metall. Mater. Trans. B Process Metall. Mater. Process. Sci. 32 (2001) 163–172.
[20] F. Miyasaka, Y. Yamane, T. Ohji, Sci. Technol. Weld. Join. 10 (2005) 521–527.
[21] J.W. Liu, Z.H. Rao, S.M. Liao, H.L. Tsai, Int. J. Heat Mass Transf. 91 (2015) 990–1000.
[22] L.L. Wang, F.G. Lu, H.C. Cui, X.H. Tang, J. Phys. D. Appl. Phys. 47 (2014) 465204.
[23] C. Cicutti, R. Boeri, Scr. Mater. 45 (2001) 1455–1460.
[24] S.A. David, J.M. Vitek, Int. Mater. Rev. 34 (1989) 213–245.
[25] R. Cao, J. Sun, J. Chen, Sci. Technol. Weld. Join. 18 (2013) 425–433.